www.small-methods.com

Suppressing Polysulfide Shuttling in Lithium-Sulfur **Batteries via a Multifunctional Conductive Binder**

Shiming Chen, Zhibo Song, Yuchen Ji, Kai Yang, * Jianjun Fang, Lu Wang, Zijian Wang, Yan Zhao, Yunlong Zhao, Luyi Yang,* and Feng Pan*

Exhibiting high specific energy and low cost, lithium-sulfur batteries are considered promising candidates for the next-generation battery. However, its wide applications are limited by the insulating nature of the sulfur, dissolution of polysulfide species, and large volume change of the sulfur cathode. In this work, a conductive binder, crosslinked polyfluorene (C-PF) is synthesized and employed in Li-S batteries to enhance the overall electrochemical performance from the following three aspects: 1) possessing high electronic conductivity, C-PF facilitates lowered areal resistance for the sulfur electrode and leads to an improved rate capability; 2) owing to the cross-linked polymer structure, favorable mechanical properties of the electrode can be achieved, hence the well-preserved electrode integrity; 3) forming strong binding with various polysulfide species, C-PF manages to trap them from diffusing to the Li anode, which greatly improves the cycling stability of Li-S cells. Through designing a multifunctional binder to comprehensively enhance the Li-S cathode, this proposed approach could be broadly applied to fully harness the energy from S redox in addition to cathode material modifications.

1. Introduction

Lithium-sulfur (Li-S) batteries have attracted tremendous research interest owing to their advantages of high specific energy, low cost, and environmental friendliness.[1-4] Despite the great progress of the reported Li-S batteries, the commercialization and large-scale application of Li-S batteries are hindered by several urgent issues: 1) the insulating nature of the sulfur and polysulfide species (e.g., Li₂S₂, Li₂S) severely limit the rate of their conversion reactions; [5,6] 2) dissolution of polysulfide into the electrolyte and the consequent shuttle effect will cause the loss of active sulfur cathode, resulting in capacity loss; [7,8] 3) large volume change of the sulfur cathode during

S. Chen, Z. Song, Y. Ji, J. Fang, L. Wang, Z. Wang, Y. Zhao, L. Yang, F. Pan School of Advanced Materials

Peking University Shenzhen Graduate School

Shenzhen 518055, P. R. China

E-mail: yangly@pkusz.edu.cn; panfeng@pkusz.edu.cn

K. Yang, Y. Zhao

Advanced Technology Institute

University of Surrey

Guildford, Surrey GU2 7XH, UK E-mail: kai.yang@surrey.ac.uk

The ORCID identification number(s) for the author(s) of this article can be found under https://doi.org/10.1002/smtd.202100839.

DOI: 10.1002/smtd.202100839

cycling not only cause the pulverization of cathode but also contact loss of the electronic pathway.[9]

Aiming to address the abovementioned challenges, different strategies have been developed to optimize the performance of Li-S batteries, especially the structure engineering of cathode[10,11] and electrolyte design.^[5] As a minor yet important component in electrodes, polymer binders have a significant effect on battery performance.[12] Through optimization of various binders, researchers have managed to immobilize the sulfur and inhibit the dissolution of polysulfides,[13-16] enhance the adhesion force to buffer the huge volume change^[17] and deliver high areal sulfur mass loading with different binder systems.[18] However, multifunctional binders that address above all issues are rarely reported.

With the progress both in experimental and computational in the synthesis for organic binder, it is now possible to design and synthesize binders with multifunctional groups.[19-21] An ideal binder for Li-S batteries should possess the following properties: 1) providing enhanced molecular interaction between polymer and polysulfides to mitigate the shuttle effect; 2) strengthening the adhesion force to maintain electrode integrity during cycling; 3) constructing a microscopic conducting pathway to boost the reaction kinetics for the insulating reactants.

Conductive binders have been reported to extend the conductive network in sulfur electrodes to enhance the rate performances while maintaining the binding function.[22,23] For electrodes with large volume changes (e.g., S, Si), binders with high resilience are equally desirable. [24,25] Therefore, in this work, a conductive binder, crosslinked polyfluorene (C-PF) is synthesized employed in Li-S batteries. As presented in Figure 1a, firstly, C-PF exhibits strong binding with polysulfide species, which largely suppresses their diffusion toward the anode. Meanwhile, possessing a much higher electronic conductivity than conventional binders (e.g., PVDF), C-PF acts as a secondary conductive network to facilitate faster electron transfer with polysulfide species bound to it. Additionally, compared with the relatively weak van der Waals forces between PVDF polymer chains, the cross-linked binder structure could also maintain the integrity of electrodes during repeated cycling despite the significant volume changes. These favorable

2366908, 2021, 1.0, Downloaded from https://onlinelibrary.wiley.com/doi/10.1002/smtd.2021010839 by University Town Of Stenzhen, Wiley Online Library on [26/11/2025]. See the Terms and Conditions (https://onlinelibrary.wiley.com/terms-and-conditions) on Wiley Online Library or rules of use; OA articles are governed by the applicable Creative Commons in the Common of the Common o

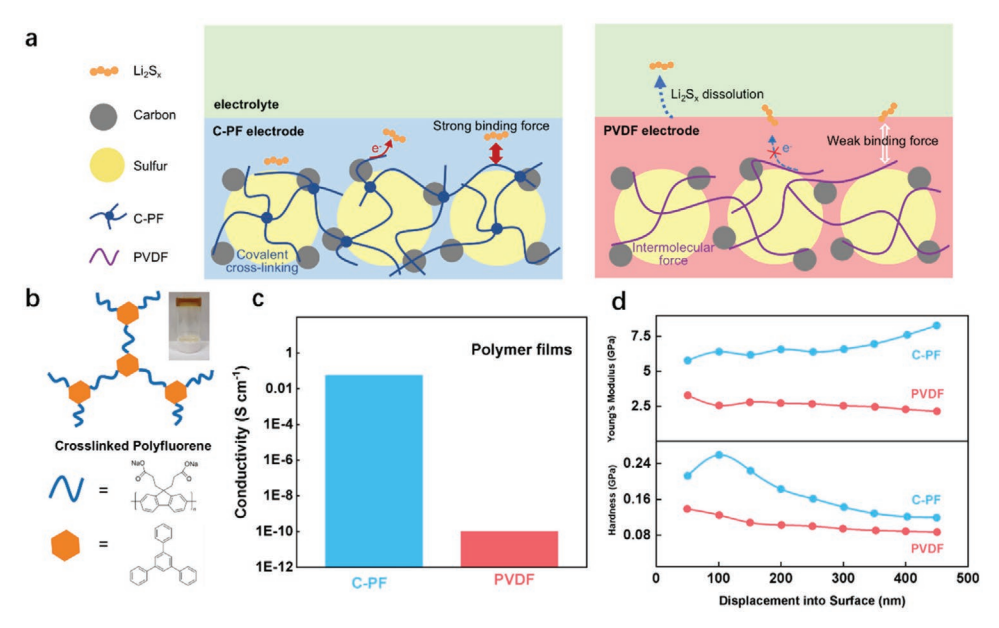


Figure 1. a) Schematic illustration of the proposed working mechanism of C-PF. b) Molecular structure of C-PF and the optical image of its aqueous solution (inset). c) Conductivity of C-PF and PVDF measured by four-point probe technique. d) Nanoindentation results of C-PF and PVDF.

properties collectively result in much-improved electrochemical performance.

2. Results and Discussion

2.1. Characterization of C-PF

The molecular structure of C-PF is presented in Figure 1b, which can be confirmed by the Fourier transform infrared spectra (Figure S2, Supporting Information), Besides, the synthesis of C-PF is schematically demonstrated in Figure S1 (Supporting Information). Owing to the solubility in water, C-PF can be easily prepared into an aqueous solution (shown in Figure 1b), allowing the electrode casting process free of environmental harmful N-dimethylformamide (NMP). For comparison, PVDF, a widely used binder in Li-S batteries, is chosen as the control group. Using the four-point probe technique, the electronic conductivity of C-PF is measured to be 5.5×10^{-2} S cm⁻¹ (Figure 1c), which is several orders of magnitude higher than PVDF $(1.0 \times 10^{-10} \text{ S cm}^{-1})$. [26] According to previous reports, the good conductivity of C-PF can be attributed to its conjugated molecular structure. [27,28] Moreover, polyfluorenes can be n-type or p-type doped under various electrochemical conditions, delivering even higher conductivity.[29,30] Nanoindentation measurement was carried out to evaluate the mechanical strength of both binders. Figure 1d shows that the C-PF film exhibits higher Young's modulus and hardness than the PVDF film which are essential to maintain the integrity of sulfur electrodes. Besides, when the deformation exceeds a certain range, Young's modulus of C-PF increases which is beneficial to restrain the collapse of the electrodes during cycling. These mechanical properties are mainly related to the degree of cross-linking which can be further tuned by changing the molar ratio of monomers. The stress-strain curve of C-PF under

tensile test is shown in Figure S3 (Supporting Information). The elastic limit of C-PF reaches 1.8 MPa which is favorable to endure the large volume expansion.

2.2. Characterization of Sulfur Electrodes

Generally speaking, due to the relatively low weight ratio of binders, their desirable properties are not necessarily reflected in electrodes. The synthesis method of S/C cathode material is shown in the Experimental Section, Figure S4 (Supporting Information) shows the SEM images of the S/C and TGA curves in Figure S5 (Supporting Information) confirmed the sulfur content in S/C was about 52.58 wt%. In order to verify this, sulfur cathodes using PVDF and C-PF as binders are fabricated (denoted as S/PVDF and S/C-PF, respectively) and characterized. The areal loadings of active materials for both electrodes are kept around 1.5 (±0.15) g cm⁻² to obtain useful conclusions. First, the areal resistivity of electrodes is measured by the four-point probe technique. Figure 2a clearly shows that the electrode using C-PF exhibits a much lower areal resistivity compared to that using PVDF. With such significant contrast, it is believed that the good electronic conductivity of C-PF contributes to the electron conduction within the electrode by forming an extended conductive network on top of conductive agents (i.e., carbon), which could provide extra reaction sites for sulfur redox and potentially mitigate the poor conductivity of sulfur and polysulfide species. Next, the electrode integrity is also crucial for sulfur cathodes due to the significant volume changes during cycling. The peeling tests (Figure 2b) clearly show that the adhesion force of S/C-PF electrode (average value = 3.034 N) is much greater than S/PVDF (average value = 1.035 N). The optical images of sulfur electrodes after peeling test are shown in Figure S6 (Supporting Information). This result suggests that S/C-PF is less likely to disintegrate owing

2366968, 2021, 1, 1). Downloaded from http://onlinelbirary.witey.com/doi/10.1002/smd.202100839 by. University Town of Stenzhen, Wiley Online Library on [26/11/2025]. See the Terms and Conditions (https://onlinelibrary.witey.com/terms-and-conditions) on Wiley Online Library for rules of use; OA articles are governed by the applicable Centwise Commons

www.advancedsciencenews.com www.small-methods.com

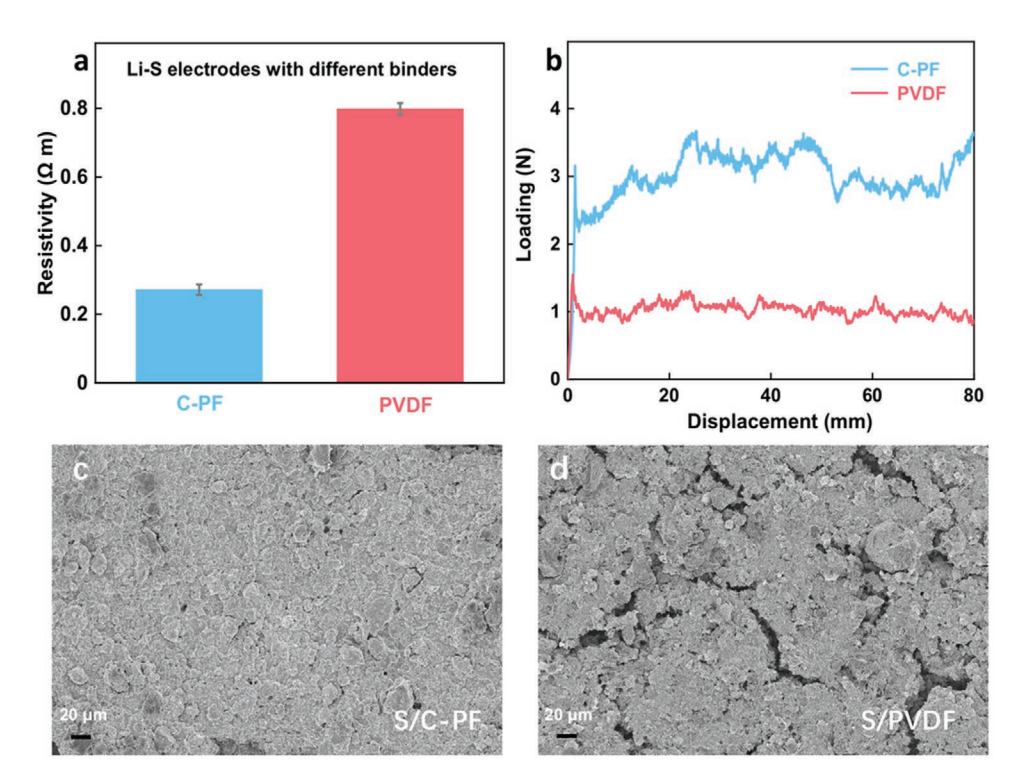


Figure 2. Characterization of sulfur electrodes using different binders. a) Resistivity and b) peeling test results of sulfur electrodes using C-PF and PVDF as binders. SEM images of sulfur electrodes using c) C-PF and d) PVDF as binders.

to the abundant polar groups (e.g., —COO¯) on C-PF, which provides strong adhesion forces with active materials as well as current collectors. [25,31,32] Scanning electron microscope (SEM) images of pristine S/PVDF (Figure 2c) and S/C-PF (Figure 2d) further confirm that C-PF enables a smooth and homogenous electrode morphology, whereas obvious cracks can be observed on the S/PVDF electrode. From these results, it can be concluded that the superior conductivity and mechanical properties of C-PF have huge impact on the pristine sulfur electrode.

2.3. Galvanostatic Cycling Performance

Next, the electrochemical performance of different cathodes is tested. Results of rate performance (Figure 3a and Figure S7, Supporting Information) show that despite showing a lower initial capacity, the cathode using C-PF possesses better rate capability than that using PVDF as binder, which could be attributed to the reduced areal resistance (Figure 2a and Figure S8, Supporting Information) of S/C-PF electrode enable by the conductive binder. The cycling stability is also evaluated (Figure 3b,c and Figure S9, Supporting Information). Under 0.1 C, S/C-PF achieved a specific capacity of 670 mAh g⁻¹ after 100 cycles, corresponding to a capacity retention of 68.4%; by sharp contrast, the capacity of S/PVDF electrodes rapidly faded to 370 mAh g-1 after 100 cycles, which is only 33.0% of the initial capacity. What is more, S/C-PF achieved a specific capacity of 480 mAh g⁻¹ after 200 cycles Under 0.5 C. The 1 C cycling performance was also improved as shown in Figure S10 (Supporting Information). It should be noted that S/C-PF

demonstrates superior cycling stability when compared with other previously reported Li-S studies focusing on binders (see Table S1, Supporting Information for detailed comparisons). To investigate the origin of the improved electrochemical performance brought by C-PF, post-mortem characterization of electrodes after cycling was carried out. From the SEM images of both electrodes (Figure 3d,e, Figure S11, Supporting Information), it can be clearly observed that the surface morphology of S/PVDF is severely fractured while the electrode integrity of S/C-PF is well preserved. This could be attributed to the adhesive property and mechanical strength of C-PF could tolerate the volume expansion/contraction of the active materials during repeated cycling, indicating a well-retained conductive network; whereas PVDF chains gradually became scattered and unable to hold the electrode together, resulting in a discontinued conductive network. In addition to the integrity of cathodes, X-ray photoelectron spectroscopy (XPS) was employed to detect whether polysulfide species have diffused to the Li anode during cycling. Characteristic peaks of Li_2S_x (x = 2-8) with high intensity are detected on the Li anode coupled with S/PVDF; by contrast, only long-chain Li_2S_x (x = 4-8) are observed on the Li anode coupled with S/C-PF.[33] In addition, the relative intensity ratio between PS species and $-SO_2/-SO_3^{2-[34,35]}$ (originated from the Li salts), indicating that polysulfide shuttling to Li anode is greatly suppressed in the presence of C-PF. Photos of the above two Li anodes (Figure S12, Supporting Information) further confirm that polysulfide shuttling towards anode is suppressed in the presence of C-PF: yellow residues (polysulfides) can only be observed on the Li anode coupled with S/PVDF while the other one is relatively clean.

2366908, 2021, 1.0, Downloaded from https://onlinelibrary.wiley.com/doi/10.1002/smtd.202100839 by University Town Of Stenzhen, Wiley Comline Library on [26/11/2025]. See the Terms and Conditions (https://onlinelibrary.wiley.com/terms-and-conditions) on Wiley Online Library or rules of use; OA articles are governed by the applicable Creative Commons is

www.advancedsciencenews.com

www.small-methods.com

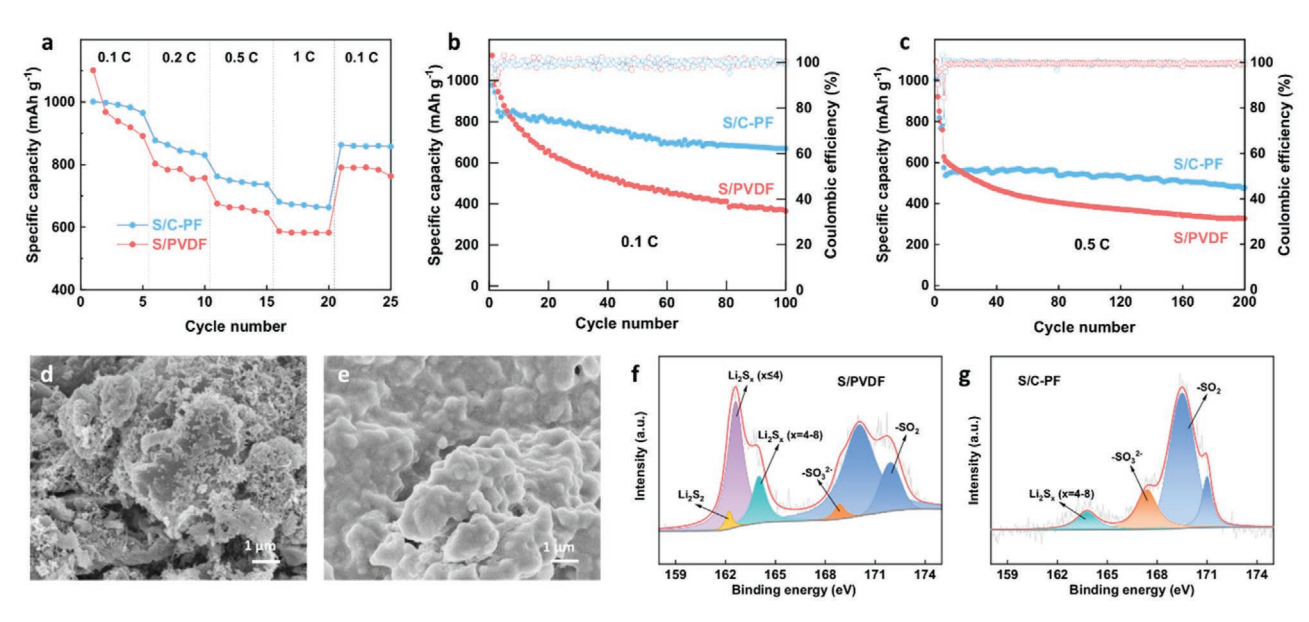


Figure 3. Electrochemical characterization of sulfur electrodes using different binders. a) Rate performance of S/C-PF and S/PVDF. Galvanostatic cycling performance of S/C-PF and S/PVDF at b) 0.1 C and c) 0.5 C after five cycles at a rate of 0.1 C. SEM images of d) S/PVDF and e) S/C-PF after cycling. S_{2p} XPS results of Li anodes coupled with f) S/PVDF and g) S/C-PF after cycling.

2.4. Trapping of Polysulfide Species

To confirm the origin of suppressed polysulfide shuttling, in situ electrochemical quartz crystal microbalance (EQCM) was employed to quantitatively and simultaneously measure the mass changes on different electrodes with different binders during the electrochemical cycling. [36,37] The frequency change of the modified crystal electrodes can be converted to the mass change in the electrodes according to the equation in Experimental Section. The cyclic voltammogram (Figure S13, Supporting Information) exhibits typical cathodic peaks around 2.3 V (vs Li/Li+), which can be assigned to the reaction of lithium ions with sulfur and the formation of polysulfides during discharging process (consistent with the CV scanning of S/C electrodes in coin-cells as shown in Figure S14, Supporting Information).^[1,5] Theoretically, the mass will continuously increase due to the lithiation process if polysulfides species are deposited on the cathode. The mass change in the S/C-PF electrode shows a more significant increase compared to S/PVDF electrode (Figure 4a), clearly indicating that polysulfide species are trapped at the cathode side by C-PF. Next, two binder films were added to two vials containing the same lithium polysulfide solution (0.005 M Li₂S₆ in DOL/DME solution), respectively and UV-vis spectra of two solutions are recorded with time. The spectra of polysulfide solution with PVDF exhibit very little change with time (24 h), which is consistent with the same solution color (Figure 4b). By sharp contrast, the intensity of absorption peaks rapidly decreased upon the addition of C-PF film (also indicated by the evident color change). The distinct difference between two solutions is attributed to that polysulfide species could firmly adsorb on C-PF films due to the strong binding effect, whereas the binding force between PVDF and polysulfide species is insufficient to facilitate such adsorption (Figure 4c). The strong adhesion force between C-PF and polysulfides is confirmed by the computational simulation results

(Figure 4d,e, Figure S15 and Table S2, Supporting Information), where much stronger binding energy ($E_{\rm binding}$) between C-PF and various polysulfide species (Li_2S_x , x=1, 2, 4, 6) can be obtained compared to PVDF. The polysulfide binding site is located on the carbonyl group of C-PF. Therefore, in addition to the high conductivity and mechanical strength, the trapping effect of C-PF on polysulfides also contributes the long cycling stability.

3. Conclusion

In this work, a conductive binder, C-PF is synthesized and employed in Li–S batteries to enhance the overall electrochemical performance from the following three aspects: 1) possessing high electronic conductivity, C-PF facilitates lowered areal resistance for the sulfur electrode and leads to improved rate capability; 2) owing to the cross-linked polymer structure, favorable mechanical properties of the electrode can be achieved, hence the well-preserved electrode integrity; 3) forming strong binding with various polysulfide species, C-PF manages to trap them from diffusing to Li anode, which greatly improves the cycling stability of Li–S cells. Through designing a multifunctional binder to comprehensively enhance the Li–S cathode, this proposed approach could be broadly applied to fully harness the energy from S redox in addition to cathode material modifications.

4. Experimental Section

Materials: The chemicals for the synthesis of polymers were purchased from Innochem or Aladdin and the tetrahydrofuran (THF) was distilled in the presence of Na with benzophenone. The compounds M1 and M2 were synthesized according to the literature. Sulfur powder was purchased from Aladdin. Carbon nanotubes (CNTs) were purchased

23669608, 2021, 10, Downloaded from https://onlinelibrary.wiley.com/doi/10.1002/smtd.202100839 by University Town Of Shenzhen, Wiley Online Library on [26/11/2025]. See the Terms and Conditions (https://onlinelibrary.wiley.

conditions) on Wiley Online Library for rules of use; OA articles are governed by the applicable Creative Commons

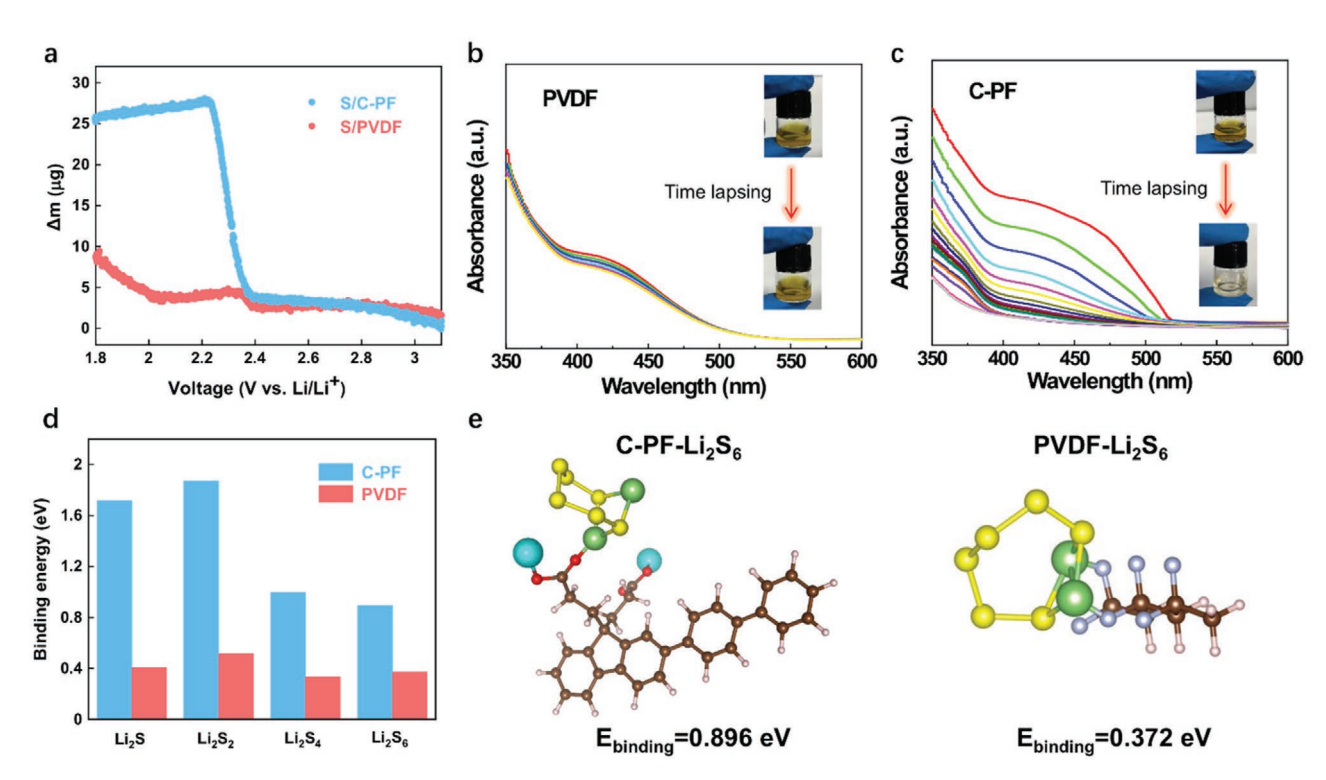


Figure 4. Characterization of suppressing effect of C-PF on polysulfide shuttling. a) EQCM tests show the mass changes of the discharging process using different binders. The scan rate is 2 mV s⁻¹ (vs Li/Li⁺). UV—vis spectra of polysulfide solution after the addition of b) PVDF and c) C-PF. d) Comparison of binding energy between different polysulfides and binders. e) Graphic example of binding between binders and Li₂S₆.

from XFNANO (Nanjing, China). The electrolyte was obtained from DoDoChem (Suzhou, China).

Synthesis of C-PF-Bu: A mixture of 2,7-dibromo-9,9-bis (3-(tert-butyl propanoate)) fluorene (M1) (4.954 g, 8.535 mmol), 2,7-bis (4,4,5,5-tetramethyl-1,3,2-dioxaborolan-2-yl)-9,9-bis (3-(tert-butyl propanoate)) fluorene (M2) (6.744 g, 10 mmol), 1,3,5-tris (4-bromophenyl)benzene (M3) (0.5296 g, 0.975 mmol), tetrakis (triphenylphosphine) palladium (0.3466 g, 0.3 mmol) and an appropriate amount of Aliquat 336 were placed in a Schlenk flask. Then distilled THF (48 mL) and Na $_2$ CO $_3$ (16 mL, 2.0 m) were added at Ar atmosphere and the mixture was stirred vigorously at 85 °C for 3 d. After the mixture was cooled down, the polymer was precipitated from dichloromethane three times, filtered, and dried under vacuum, receiving 83% yield.

Synthesis of C-PF: C-PF-Bu was dissolved in dichloromethane solution with 15 wt% trifluoroacetic acid in a mass ratio of 1:40. The mixture was stirred at room temperature overnight. The solvent was removed under reduced pressure after the reaction stopped, resulting in a yellow residue. The residue was treated with aqueous NaOH (1 M) solution and purified by dialysis against deionized water for 3 d. Finally, the purified solution was free-dried to get C-PF with 72% yield.

Material Characterizations: Field-emission scanning electron microscopy (ZEISS SUPRA55, Carl Zeiss) was used to observe the topview morphology of as-prepared samples. Fourier transform infrared (FTIR) spectra were collected on a Nicolet Avatar 360 spectrophotometer (ATR) and the absorption of radiation in the UV-vis region was continuously measured by SHIMADZU UV-2450. X-ray photoelectron spectra (XPS) were collected by ESCALAB 250Xi. The conductivity of polymer films was measured by Keithley 4200-SCS semiconductor characterization system and probe station (PS-100, Lakeshore) at room temperature in ambient air.

Peeling tests of the S/C electrodes were conducted on a microcomputer-controlled electronic universal testing machine (MDTC-EQ-M12-01). The electrode samples were cut into strips of 20×60 mm. Then both sides of the samples were attached to 3M 600 Scotch tapes (20 mm in width) with an opening at one end. The free ends of 3M tapes

were attached to the machine grips. The electrodes were pulled by the Scotch tapes at the angle of 180° at a constant displacement rate of 60 mm min⁻¹ to peel off the aluminum current collector. The applied force was continuously measured and the balance plateau values of force were collected.

Four gold electrodes (2 mm \times 2 mm) were vacuum deposited on the surface of the polymer films before the electric conductivity was measured. The distance between two gold electrodes is 5 mm. The conductivities were measured by a four-probe method which was calculated from their measured sheet resistances and exact film thickness. The internal resistance (AC-IR) of electrodes was measured using HIOKI 3561 battery HiTester. Under a pressure of 10 MPa, the electrode plate (diameter = 4 cm) was clamped by a pair of coppery terminals for 30 s during testing. The thickness of plates was obtained by a micrometer caliper. Then the resistivity was calculated through the formula $\rho = RS/L$ and the mean value and standard deviation were demonstrated.

Adsorption Test of Lithium Polysulfide: The binders were dried under vacuum at 60 °C overnight before the adsorption test. 1 M Li₂S₆ was synthesized by mixing sulfur and Li₂S in DOL/DME solution (1:1, v/v). Then the solution was stirred at 70 °C in an argon-filled glove box for 8 h. The color of the solution turned brownish red. The Li₂S₆ solution was diluted to 0.005 M for the polysulfide adsorption test.

Preparation of Electrodes: The acetylene black carbon (ABC), activated carbon (AC), carbon nanotubes (CNTs), and sublimed sulfur powder (a mass ratio of 3:1:1:5) were mixed ground and ball-milled for 1 h. The mixture was transferred to a sealed hydrothermal kettle and heated at 155 °C overnight to obtain the S/C composite. [38] The TGA curves in Figure S5 (Supporting Information) show the mass content of sulfur in S/C composite. And the SEM images of S/C material are shown in Figure S4 (Supporting Information). All working electrodes were prepared by active materials (S/C) and binder (C-PF or PVDF) at a mass ratio of 9:1 with a typical slurry casting method. The slurry was cast onto Al foil and dried at room temperature, followed by drying at 60 °C under vacuum and cutting into disks with a diameter of 10 mm. The average areal

www.advancedsciencenews.com

www.small-methods.com

small methods

2366908, 2021, 1.0, Downloaded from https://onlinelibrary.wiley.com/doi/10.1002/smtd.2021010839 by University Town Of Stenzhen, Wiley Online Library on [26/11/2025]. See the Terms and Conditions (https://onlinelibrary.wiley.com/terms-and-conditions) on Wiley Online Library or rules of use; OA articles are governed by the applicable Creative Commons in the Common of the Common o

loading of active materials on each electrode was about 1.5 mg cm $^{-2}$. Two-electrode CR2032 coin-type half-cells were assembled in an argon-filled glove box with lithium foils as the counter and reference electrodes, S/C as working electrodes. 1.0 M LiTFSI in 1:1 (v/v) DME/DOL with 2% LiNO₃ was used as the electrolyte and the separator was porous PP films (Celgard 2400).

Electrochemical Measurements: The galvanostatic cycling and rate capability tests were carried out using a Neware battery test system (Newell, China) within the voltage range of 1.6–2.7 V (vs Li/Li⁺). EIS experiments were performed on a CHI 604E electrochemical station with a frequency range of 1 M Hz to 0.1 Hz.

EQCM measurements were performed by a quartz crystal microbalance (QCM922) in conjunction with a VersaSTAT 3 Galvanostat/Potentiostat. The working electrodes were prepared by coating the goad-coated quartz crystals (reference frequency of 9 MHz) with S/C slurry (as mentioned in Preparation of electrodes) and drying under 80 °C, leading to an areal mass loading of 0.2 mg cm⁻². Lithium wire was used as counter and reference electrodes. The EQCM experiments were measured in the voltage range 1.8 to 3.1 V (vs Li/Li⁺) at a scan rate of 1 mV s⁻¹. The mass change during the electrochemical reaction is calculated as the following formula:

$$\Delta f = -\frac{2f_0^2}{A\sqrt{\mu_0\rho_0}}\Delta m\tag{1}$$

where Δf shows the frequency change of the gold-coated quartz crystal electrode; f_0^2 denotes the resonant frequency of the quartz crystal; A is the active crystal surface; $\mu_{\rm Q}$ is the shear modulus of quartz (2.947 \times 10¹¹ g cm⁻¹ s⁻²); the last term $\rho_{\rm Q}$ is the density of quartz (2.648 g cm⁻³).

DFT Calculations: All calculations were based on the Gaussian 09 package [39] by the density functional theory (DFT) method. Besides, m062x [40]/6-311G***[41] theory level was used to optimize the molecular structure and calculate the binding energies of polysulfide. The split-valence-shell Gaussian basis set 6-311G** was used for the C, H, O, F, S, Li, and Na atoms. Vesta software was used to draw the Structural diagram. The binding energy (ΔE_{bind}) was used to measure the binding strength between the Li₂S_n (Li₂S, Li₂S₂, Li₂S₄, Li₂S₆) species and the polymer X (PVDF/C-PF). The ΔE_{bind} was defined by:

$$\Delta E_{\text{bind}} = E_{\text{Li}_2 S_n + X} - E_{\text{Li}_2 S_n} - E_X + E_{\text{bsse}} (n = 1, 2, 4, 6)$$
 (2)

where the $E_{\text{Li}_2S_n}$ and E_X are the energies of isolated Li_2S_n species and polymer X calculated at their states; the $\text{E}_{\text{Li}_2S_n+X}$ denotes the total energy of the Li_2S_n/X adsorbed system; the last term E_{bsse} is the energy of the basis set superposition error which was obtained by using the counterpoise method.

Supporting Information

Supporting Information is available from the Wiley Online Library or from the author.

Acknowledgements

S.C., Z.S., and Y.J. contributed equally to this work. This work was financially supported by the National Key R&D Program of China (2016YFB0700600), China Postdoctoral Science Foundation (2019M660317).

Conflict of Interest

The authors declare no conflict of interest.

Data Availability Statement

Research data are not shared.

Keywords

conductive binder, lithium-sulfur batteries, mechanical stability, polysulfide trapping, shuttle effect

Received: July 21, 2021 Revised: August 31, 2021 Published online: September 9, 2021

- [1] Q. Guo, Z. Zheng, Adv. Funct. Mater. 2020, 30, 1907931.
- [2] M. Winter, B. Barnett, K. Xu, Chem. Rev. 2018, 118, 11433.
- [3] Z. Zheng, H. H. Wu, H. Liu, Q. Zhang, X. He, S. Yu, V. Petrova, J. Feng, R. Kostecki, P. Liu, D. L. Peng, M. Liu, M. S. Wang, ACS Nano 2020, 14, 9545.
- [4] P. G. Bruce, S. A. Freunberger, L. J. Hardwick, J. M. Tarascon, Nat. Mater. 2012, 11, 19.
- [5] H. Yuan, J. Q. Huang, H. J. Peng, M. M. Titirici, R. Xiang, R. Chen, Q. Liu, Q. Zhang, Adv. Energy Mater. 2018, 8, 1802107.
- [6] L. Ji, M. Rao, S. Aloni, L. Wang, E. J. Cairns, Y. Zhang, Energy Environ. Sci. 2011, 4, 5053.
- [7] A. Manthiram, Y. Fu, S. H. Chung, C. Zu, Y. S. Su, Chem. Rev. 2014, 114, 11751.
- [8] A. Raulo, S. Bandyopadhyay, S. Ahamad, A. Gupta, R. Srivastava, P. Formanek, B. Nandan, J. Power Sources 2019, 431, 250.
- [9] E. T. Kim, J. Park, C. Kim, A. G. Simmonds, Y. E. Sung, J. Pyun, K. Char, ACS Macro Lett. 2016, 5, 471.
- [10] M. Wang, X. Xia, Y. Zhong, J. Wu, R. Xu, Z. Yao, D. Wang, W. Tang, X. Wang, J. Tu, Chem. - Eur. J. 2019, 25, 3710.
- [11] Y. Wang, T. Yin, Z. Su, C. Qiu, Y. Wang, R. Zheng, M. Chen, X. Shuai, Nano Res. 2018, 11, 3710.
- [12] K. Yang, L. Yang, Z. Wang, B. Guo, Z. Song, Y. Fu, Y. Ji, M. Liu, W. Zhao, X. Liu, S. Yang, F. Pan, Adv. Energy Mater. 2021, 11, 2100601.
- [13] P. D. Frischmann, Y. Hwa, E. J. Cairns, B. A. Helms, Chem. Mater. 2016, 28, 7414.
- [14] J. Guo, Z. Yang, Y. Yu, H. D. Abruña, L. A. Archer, J. Am. Chem. Soc. 2013, 135, 763.
- [15] G. Li, M. Ling, Y. Ye, Z. Li, J. Guo, Y. Yao, J. Zhu, Z. Lin, S. Zhang, Adv. Energy Mater. 2015, 5, 1500878.
- [16] B. A. Trofimov, L. v. Morozova, M. v. Markova, A. I. Mikhaleva, G. F. Myachina, I. v. Tatarinova, T. A. Skotheim, J. Appl. Polym. Sci. 2006, 101, 4051.
- [17] D. He, P. Li, W. Wang, Q. Wan, J. Zhang, K. Xi, X. Ma, Z. Liu, L. Zhang, X. Qu, Small 2020, 16, 1905736.
- [18] H. Yi, Y. Yang, T. Lan, T. Zhang, S. Xiang, T. Tang, H. Zeng, C. Wang, Y. Cao, Y. Deng, ACS Appl. Mater. Interfaces 2020, 12, 29316.
- [19] R. Fayt, R. Jerome, P. Teyssié, Makromol. Chem. 1986, 187, 837.
- [20] J. T. Li, Z. Y. Wu, Y. Q. Lu, Y. Zhou, Q. sen Huang, L. Huang, S. G. Sun, Adv. Energy Mater. 2017, 7, 1701185.
- [21] M. J. Lacey, F. Jeschull, K. Edström, D. Brandell, J. Phys. Chem. C 2014, 118, 25890.
- [22] G. Ai, Y. Dai, Y. Ye, W. Mao, Z. Wang, H. Zhao, Y. Chen, J. Zhu, Y. Fu, V. Battaglia, J. Guo, V. Srinivasan, G. Liu, *Nano Energy* 2015, 16, 28.
- [23] L. Yan, X. Gao, F. Wahid-Pedro, J. T. Ernest Quinn, Y. Meng, Y. Li, J. Mater. Chem. A 2018, 6, 14315.
- [24] F. Zou, A. Manthiram, Adv. Energy Mater. 2020, 10, 2002508.
- [25] J. Liu, D. G. D. Galpaya, L. Yan, M. Sun, Z. Lin, C. Yan, C. Liang, S. Zhang, Energy Environ. Sci. 2017, 10, 750.



methods

23669608, 2021, 10, Downloaded from https://onlinelibrary.wiley.com/doi/10.1002/smtd.202100839 by University Town Of Shenzhen, Wiley Online Library on [26/11/2025]. See the Terns

and Condition

of use; OA

are governed by the applicable Creative Commons

www.advancedsciencenews.com www.small-methods.com

- [26] B. T. S. Ramanujam, C. Gopalakrishnan, Bull. Mater. Sci. 2021, 44, 66.
- [27] Y. Zhao, L. Yang, Y. Zuo, Z. Song, F. Liu, K. Li, F. Pan, ACS Appl. Mater. Interfaces 2018, 10, 27795.
- [28] D. Liu, Y. Zhao, R. Tan, L. L. Tian, Y. Liu, H. Chen, F. Pan, Nano Energy 2017, 36, 206.
- [29] T. W. Kwon, J. W. Choi, A. Coskun, Chem. Soc. Rev. 2018, 47, 2145.
- [30] Y. Lee, S. Y. Kim, D. Y. Kim, S. Lee, Nanomaterials 2020, 10, 1486.
- [31] Q. Zhang, C. Zhang, W. Luo, L. Cui, Y. J. Wang, T. Jian, X. Li, Q. Yan, H. Liu, C. Ouyang, Y. Chen, C. L. Chen, J. Zhang, Adv. Sci. 2020, 7, 2000749.
- [32] H. Chen, M. Ling, L. Hencz, H. Y. Ling, G. Li, Z. Lin, G. Liu, S. Zhang, Chem. Rev. 2018, 118, 8936.
- [33] Y. X. Song, Y. Shi, J. Wan, S. Y. Lang, X. C. Hu, H. J. Yan, B. Liu, Y. G. Guo, R. Wen, L. J. Wan, Energy Environ. Sci. 2019, 12, 2496.
- [34] M. I. Nandasiri, L. E. Camacho-Forero, A. M. Schwarz, V. Shutthanandan, S. Thevuthasan, P. B. Balbuena, K. T. Mueller, V. Murugesan, *Chem. Mater.* 2017, 29, 4728.
- [35] Y. Diao, K. Xie, S. Xiong, X. Hong, J. Electrochem. Soc. 2012, 159, A1816.
- [36] T. Liu, L. Lin, X. Bi, L. Tian, K. Yang, J. Liu, M. Li, Z. Chen, J. Lu, K. Amine, K. Xu, F. Pan, Nat. Nanotechnol. 2019, 14, 50.

- [37] K. Yang, Y. Li, L. Jia, Y. Wang, Z. Wang, Y. C. Ji, S. Yang, M. Titirici, X. Liu, L. Yang, F. Pan, J. Energy Chem. 2021, 56, 438.
- [38] R. Fang, H. Xu, B. Xu, X. Li, Y. Li, J. B. Goodenough, Adv. Funct. Mater. 2021, 31, 2001812.
- [39] M. J. Frisch, G. W. Trucks, H. B. Schlegel, G. E. Scuseria, M. A. Robb, J. R. Cheeseman, G. Scalmani, V. Barone, G. A. Petersson, H. Nakatsuji, X. Li, M. Caricato, A. Marenich, J. Bloino, B. G. Janesko, R. Gomperts, B. Mennucci, H. P. Hratchian, J. V. Ortiz, A. F. Izmaylov, J. L. Sonnenberg, D. Williams-Young, F. Ding, F. Lipparini, F. Egidi, J. Goings, B. Peng, A. Petrone, T. Henderson, D. Ranasinghe, V. G. Zakrzewski, J. Gao, N. Rega, G. Zheng, W. Liang, M. Hada, M. Ehara, K. Toyota, R. Fukuda, J. Hasegawa, M. Ishida, T. Nakajima, Y. Honda, O. Kitao, H. Nakai, T. Vreven, K. Throssell, J. A. Montgomery Jr., J. E. Peralta, F. Ogliaro, M. Bearpark, J. J. Heyd, E. Brothers, K. N. Kudin, V. N. Staroverov, T. Keith, R. Kobayashi, J. Normand, K. Raghavachari, A. Rendell, J. C. Burant, S. S. Iyengar, J. Tomasi, M. Cossi, J. M. Millam, M. Klene, C. Adamo, R. Cammi, J. W. Ochterski, R. L. Martin, K. Morokuma, O. Farkas, J. B. Foresman, D. J. Fox, Gaussian 09, Revision A.02, Gaussian, Inc., Wallingford CT, 2016.
- [40] Y. Zhao, D. G. Truhlar, Theor. Chem. Acc. 2008, 120, 215.
- [41] M. J. Frisch, J. A. Pople, J. S. Binkley, J. Chem. Phys. 1984, 80, 3265.